Asphaltene-induced spontaneous emulsification: Effects of interfacial co-adsorption and viscoelasticity

Mariana Rodríguez-Hakim, Satyam Anand, Javier Tajuelo, Zhen Yao, Aadithya Kannan, and Gerald G. Fuller

Citation: Journal of Rheology **64**, 799 (2020); doi: 10.1122/1.5145307
View online: https://doi.org/10.1122/1.5145307
View Table of Contents: https://sor.scitation.org/toc/jor/64/4
Published by the The Society of Rheology

Asphaltene-induced spontaneous emulsification: Effects of interfacial co-adsorption and viscoelasticity

Mariana Rodríguez-Hakim,[1] Satyam Anand,[2] Javier Tajuelo,[1,3] Zhen Yao,[4] Aadithya Kannan,[1] and Gerald G. Fuller[1,a)]

[1]*Department of Chemical Engineering, Stanford University, Stanford, California 94305*
[2]*Department of Chemical Engineering, Indian Institute of Technology Delhi, New Delhi 110016, Delhi, India*
[3]*Departamento de Física Interdisciplinar, Universidad Nacional de Educación a Distancia, UNED, 28040 Madrid, Spain*
[4]*Institute of Polymerization and Polymer Engineering, Zhejiang University, Hangzhou, Zhejiang 310027, People's Republic of China*

(Received 16 January 2020; final revision received 20 April 2020; published 7 May 2020)

Abstract

Asphaltenes are a class of high molecular weight aromatic compounds found in crude oil. They adsorb onto toluene-water interfaces and induce a spontaneous emulsification phenomenon, whereby stable water-in-oil emulsions form without the need of an external energy input. This work aims to control and understand the factors affecting spontaneous droplet formation in the presence of asphaltene adsorption. This is particularly useful for crude oil refining, where the presence of a stable emulsion hampers the efficiency of downstream processing operations. We explore the effect of the addition of copolymers designed as crude oil flow improvers as a means to control the extent of emulsion formation. We find that the polymers competitively adsorb onto the toluene-water interface and diminish spontaneous emulsification. We also conduct fluorescence microscopy experiments and measurements of the interfacial energy to determine the mechanism of spontaneous emulsification in asphaltene systems. We conclude that an emulsion forms via the diffusion of molecular water into the oil phase and subsequent binding with asphaltene aggregates, leading to the nucleation of micrometer-sized water droplets. We find that the polymer forms complexes with the dissolved asphaltenes, possibly hampering the ability of diffused water to bind to the asphaltenes and reducing the extent of spontaneous emulsification. Finally, we investigate the role of interfacial shear and dilatational viscoelasticity to better understand which fundamental interfacial properties are important in the emulsification of asphaltene-laden systems. We find that the rate of formation of an interfacial microstructural network is inversely correlated with the extent and rate of spontaneous emulsification. https://doi.org/10.1122/1.5145307

I. INTRODUCTION

Traditionally, emulsions are thought of as thermodynamically unstable systems formed when one liquid phase is dispersed in a second immiscible liquid [1]. Most emulsions require a large input of mechanical energy to be formed, since the work required to increase the surface area of an interface is proportional to the product between the interfacial tension, γ, and the surface area. Thus, if drop sizes are small (typically between hundreds of nanometers and tens of micrometers) or the interfacial tension is high, a greater amount of mechanical energy needs to be supplied [2].

In practice, the free energy of emulsion formation is reduced through the addition of surface active emulsifiers such as surfactants, polymers, or nanoparticles [3]. For instance, surfactants reduce the surface energy of an interface by decreasing the energy gap between an emulsified state and a phase separated state [3]. On the other hand, the lifetime of an emulsion can be increased by adding polymers that adsorb onto the liquid-liquid interface and render it more rigid, thus decreasing the tendency for coalescence and increasing emulsion stability [4]. Although these strategies facilitate the emulsion forming process, over time the emulsion will once again phase separate and adopt a thermodynamically stable configuration [3,4].

Although most systems require intense mechanical agitation in order to be emulsified, there exists a special kind of emulsion that can form without the need of an external energy input [1]. These "spontaneous emulsions" represent thermodynamically stable configurations in which the total system free energy is at a minimum [2,5]. They require the presence of one or multiple types of surface active components that adsorb at the droplet interface separating the immiscible liquid phases and can produce droplets of vastly different sizes ranging from hundreds of nanometers to tens of micrometers [2].

The "ouzo effect" is one of the most common examples of spontaneous emulsification and occurs when water is added to anise-flavored alcoholic beverages such as ouzo, raki, or absinthe [6]. The hydrophobic oils dissolved in these liquors aggregate into small droplets, which are stabilized by ethanol and dispersed in an aqueous continuous phase [6]. The resulting oil-in-water emulsion contains droplets on the order of 100 nm in size, which refract light and render the beverage a cloudy white color. The same effect is seen in ternary systems composed of benzene, ethyl acetate, and water [7] and toluene, propionic acid, and water [8].

a)Author to whom correspondence should be addressed; electronic mail: ggf@stanford.edu

Spontaneous emulsification can also occur during the extraction and processing of crude oil [9,10]. It has been found that droplets of water, between 5 and 20 μm in size, can spontaneously appear when crude oil is put into contact with water [9]. These water-in-oil emulsions can cause problems during downstream processing, leading to ineffective phase separation during crude oil desalting and subsequent pipe corrosion [9–13].

A study conducted by Bochner de Araujo *et al.* found that natural surfactants in crude oil, such as asphaltenes, adsorb onto oil-water interfaces and are responsible for the spontaneous emulsification process [9]. In this study, a model oil system composed of toluene with different fractions of dissolved asphaltenes was gently put into contact with water; over time, asphaltene-laden water droplets were seen to form near the vicinity of the oil-water interface [9]. Thus, a fundamental understanding of the spontaneous emulsification process in the presence of asphaltene adsorption is of key importance for controlling the rate and extent of droplet formation and thus improving the efficiency of oil extraction operations.

The aforementioned studies have unequivocally demonstrated that asphaltenes can induce a spontaneous emulsification phenomenon upon adsorption to toluene-water interfaces. However, several important questions still remain. For one, it is unclear whether the rate and extent of this emulsion forming process can be practically controlled. Several studies have been carried out in which the stability of water-in-oil emulsions has been manipulated through the addition of low concentrations of demulsifiers [12,14,15]; however, many of these studies have been conducted with mechanically generated emulsions, whose energetics and dynamics strongly differ from those of spontaneous emulsions.

Second, even though a minimization of the free energy can explain why spontaneously emulsified systems are stable, it does not explain how spontaneous emulsification occurs. Three main mechanisms have been proposed, each of which is valid in different systems and produce droplets of different sizes [2,5,8]. Two of the mechanisms, interfacial turbulence and interfacial bending, are produced via a mechanical breakup of the interface [2]. The third mechanism, termed diffusion and stranding, results from a jump in chemical potential across the interface [8,16].

A recent study by Duboué *et al.* investigated the mechanism responsible for spontaneous emulsification in an asphaltene-toluene-water system [10]. They reported the appearance of a water-in-oil emulsion in a system consisting of an asphaltene-in-toluene solution in contact with a saturated water vapor. They also conducted experiments in which fluorescent dyes were introduced into the toluene and water phases, where they reported the absence of dye within the spontaneously formed droplets. These two experiments led the authors to suggest that a mechanism akin to diffusion and stranding was responsible for spontaneous emulsification in the presence of asphaltenes. However, they did not investigate or rule out the remaining two mechanisms, for which further analysis is needed.

Finally, even though the role of interfacial viscoelasticity has been deemed to be the main factor contributing to the long-term stability of asphaltene-coated droplets [11,12,17], a thorough study of the role of interfacial viscoelasticity in spontaneous emulsification has not yet been conducted. A recent study by Bochner de Araujo *et al.* reveals that the rate of shrinkage of a millimeter-sized spherical water drop suspended in toluene at a specified asphaltene concentration due to spontaneous emulsification is only dependent on the drop's initial radius [13]. Thus, once a spherical drop is formed, it will always shrink at a constant rate that is independent of its current size. These results suggest that interfacial aging and the development of a viscoelastic network decrease the rate of spontaneous emulsification; however, the influence of the mode of deformation (shear or dilatational) has not yet been investigated.

The goal of the present study is to control and understand spontaneous droplet formation in the presence of asphaltenes. This is accomplished by means of three different aims. First, we investigate the use of polymeric flow improvers as a means to control the rate and the extent of spontaneous emulsification. Using brightfield microscopy, we quantify the degree of spontaneous emulsification for different working solutions and show that the addition of the polymer can almost entirely suppress this phenomenon in the presence of asphaltenes. These polymers not only deliver a practical means to suppress undesired emulsion formation but also provide a reference platform to understand which fundamental interfacial properties are important in the emulsification of asphaltene-laden systems.

Second, we provide a thorough overview of the three different mechanisms of spontaneous emulsification. We then show, via fluorescence microscopy and measurements of the interfacial energy, that diffusion and stranding are the mechanisms responsible for spontaneous emulsification in asphaltene-coated interfaces, confirming the results presented by Duboué *et al.* [10]. We conduct small-angle x-ray scattering (SAXS) experiments and show that the polymer forms complexes with the dissolved asphaltenes, which can act to suppress emulsification.

Finally, we characterize the viscoelastic response of asphaltene and polymer interfaces under shear and dilatational deformations. Although spontaneous emulsification is produced via diffusion of molecular water and is independent of the magnitude of the interfacial energy, we find that interfacial viscoelasticity is inversely proportional to the rate of spontaneous emulsification. Asphaltene-only interfaces exhibit a gradual buildup of interfacial viscoelasticity—as the interfacial network develops, the rate of emulsification decreases. On the other hand, interfaces that are capable of rapidly building a strong interfacial microstructure, such as those that contain the polymer, can quickly suppress emulsification.

II. MATERIALS AND METHODS

A. Asphaltene and polymer solutions

Asphaltenes are a class of polycyclic aromatic compounds found in crude oil. They comprise the fraction of crude oil that is soluble in toluene and insoluble in n-heptane and thus do not have a fixed molecular structure [18,19]. A typical

asphaltene molecule has between 6 and 10 fused aromatic rings surrounded by aliphatic side chains [18–20] and can contain a few charged or polar heteroatoms such as N, O, and S [21]. Although highly polydisperse, their average molecular weight is around 750 g/mol [19].

Asphaltene molecules typically form nanoaggregates of ~ 10 molecules when their concentration in toluene solution exceeds the critical nanoaggregate concentration (CNAC) of approximately 0.1 mg/ml [19,22,23]. These nanoaggregates can, in turn, assemble into colloidal-scale clusters with dimensions between 6 and 10 nm [19,20]. Neutron scattering experiments [23] and molecular dynamics (MD) simulations [21] have revealed that asphaltenes adsorb as clusters at toluene-water interfaces. Specifically, the MD simulations show that although asphaltenes partition completely into the toluene phase, those with charged side groups remain strongly tethered to the toluene-water interface via hydrogen bonding with the aqueous phase [21].

The asphaltenes used in this study were extracted from an oil field of the China Petroleum & Chemical Corporation (also known as Sinopec) and provided to us by the Shanghai Research Institute of Petrochemical Technology, which is an R&D affiliate of Sinopec. The asphaltenes were separated from the crude oil via a modification of the ASTM D2007-03 method [24]. Further details of the separation and purification process can be found in [25]. An elemental composition analysis of the extracted asphaltenes was conducted by Cao *et al.* in [26], which revealed that the asphaltenes contain 1.47 wt. % N and 3.74 wt. % S. The resulting Fourier-transform infrared spectrum also shows the presence of hydroxyl and amine groups, suggesting that asphaltenes are capable of attaching to the oil/water interface and forming hydrogen bonds with the bulk water phase. The solid asphaltenes were dissolved in anhydrous toluene (Fisher Chemicals, water content $<0.001\%$) at a concentration of 1 mg/ml. The solution was stirred until all visible asphaltene flocs were dissolved.

Polymeric flow improvers have been used to pretreat crude oils in order to improve flowability and decrease crystallization [25–27]. A series of papers by the Yao group at Zhejiang University discuss the synthesis of a custom copolymer, poly(styrene-alt-octadecyl maleimide) or (*alt*) SNODMI, hereafter referred to as a polymer [25–27]. They show that polymer concentrations as low as 0.1 wt. % in model crude oils can successfully reduce the size of waxy crystals, crystallization temperature, yield stress, and solution viscosity of crude oils with and without dissolved asphaltenes [25].

Since the use of (*alt*)SNODMI has already been proven to be advantageous in crude oil processing, it is reasonable to assume that it may also have the added benefit of inhibiting the spontaneous emulsification of asphaltene-toluene systems with water. A polymer sample with a molecular weight of 3500 g/mol and an imidization degree of 100% [27] was used as an emulsification inhibitor in our studies. Solutions of polymer in toluene were prepared by dissolving different mass fractions (between 0.25% and 2.00%) of the copolymer with either pure toluene or a 1 mg/ml asphaltene-in-toluene solution.

All asphaltene and/or polymer solutions were sonicated for 30 min prior to the start of each experiment. For all experiments, filtered de-ionized (DI) water was used as the aqueous phase.

B. Brightfield microscopy

Brightfield microscopy studies of asphaltene and/or polymer-laden interfaces were conducted using a Nikon Ti2-E inverted microscope. A 20× air objective is used to vertically scan the oil/water interface. A glass cell is built by glueing a cylindrical capillary (5 mm diameter by 10 mm height) to a glass coverslip with a thickness of 0.1 mm. Prior to each experiment, the chamber is plasma treated to render the glass hydrophilic and ensure the presence of smooth contact lines that facilitate imaging.

At the start of each experiment, 10 µl of DI water is injected into the chamber using a glass syringe, making sure that the bottom of the chamber is completely covered in water. The chamber is positioned onto the microscope stage, and the center of the water-air meniscus is located. Once the horizontal position of the objective is in place, 20 µl of the asphaltene and/or polymer solution is injected into the chamber using a separate glass syringe. The chamber is immediately covered using a glass slide to prevent evaporation. The water-toluene interface is located through the presence of spontaneously emulsified drops. Videos of the interface are recorded for 1-min intervals immediately after the interface is located (0 min) and then after 4, 10, 20, 40, and 60 min.

C. Fluorescence microscopy

Fluorescence microscopy studies were conducted using a Nikon TiE inverted spinning disk confocal microscope. A 40× water-immersed objective is used to vertically scan the interface between fluorescently labeled water and asphaltene-toluene solutions. The experimental protocol is the same as described in Sec. II B, with the exception that now the oil and water phases contain dissolved flourophores. Images are recorded at different focal planes (z-stack), moving vertically upward from the bulk water phase, across the liquid-liquid interface, and into the bulk oil phase. This process is repeated three times for the brightfield channel, the hydrophilic fluorophore laser, and the hydrophobic fluorophore laser. After acquisition is complete, the z-stacks are postprocessed using the Fiji image-processing software.

Similar experiments with asphaltene solutions have been previously carried out by Bochner *et al.* [9] using fluorescein and Nile red to fluorescently label the aqueous and oleic phases, respectively. A different set of dyes was selected for the present study since fluorescein's excitation wavelength overlaps with the adsorption wavelength of the asphaltene solution, potentially damping the fluorescent signal emitted by the aqueous droplets.

A spectrophotometer was used to scan the absorption profiles of asphaltene-in-toluene solutions at different concentrations ranging from 0.125 to 1 mg/ml (see the supplementary material [54] for spectra). Although asphaltenes absorb visible light, absorption in the near IR region is minimized.

Thus, a near IR water-soluble fluorophore, sulfocyanine 5.5 carboxylic acid or SC5.5 (Lumiprobe) with a concentration of 6 ng/ml, was selected. For the oil phase, an asphaltene concentration of 0.25 mg/ml was used to further mitigate the attenuation of the aqueous fluorescent signal in the oil phase. A toluene-soluble fluorophore, BDP FL azide or BDP (Lumiprobe) at a concentration of 75 ng/ml, was chosen such that its emission and excitation wavelengths would not overlap with those of the aqueous dye.

A control experiment was carried out in which a 2:1 ratio of asphaltene/BDP/toluene to SC5.5/water was introduced into a sealed glass vial and vigorously agitated to mechanically create an emulsion. The emulsion was imaged under the microscope, revealing the existence of fluorescently tagged water droplets suspended in a fluorescently tagged oil medium. This reveals that the signal from the aqueous fluorophore is not attenuated by the oil phase and that fluorescent dye present inside an emulsified droplet is indeed visible. Images from the control experiment are included in the supplementary material [54].

D. Small-angle x-ray scattering

SAXS is a technique that uses x rays to probe material structures and determines the particle size in the submicrometer range. The SAXS measurements reported in this study have been conducted using beamline 1-5 at the Stanford Synchrotron Radiation Lightsource, a division of the SLAC National Accelerator Laboratory (Stanford, CA). Two different oil solutions were prepared using the materials outlined in Sec. II A: 1 mg/ml asphaltene in toluene and 1 mg/ml asphaltene + 2.00% polymer in toluene. The samples appear homogeneous, and no visible flocs or precipitation are observed. The samples are introduced inside cylindrical glass capillaries and measured at 23 °C with an exposure time of 120 s. The synchrotron x-ray energy was 15 keV. The scattering intensity I is obtained as a function of q, where q is the scattering wavevector. The data are analyzed using the Irena and Nika packages in IGOR, a data analysis and plotting software, to obtain a length scale corresponding to the radius of gyration of the asphaltene and/or asphaltene + polymer structures.

E. Interfacial tension—Pendant drop tensiometry

Pendant drop tensiometry is a common and robust technique for measuring the interfacial energy of liquid-liquid or liquid-air interface [28,29]. In this method, a pendant drop is formed on a capillary and its shape is iteratively fit to the Young–Laplace equation to obtain a single scalar value for the interfacial tension [28,29].

Although complex interfaces are described by a position-dependent interfacial energy tensor, as seen in Sec. III A, there are cases where γ reduces to a constant scalar value, rendering traditional shape-fitting methods valid for the interfacial energy calculation. This can be achieved in complex interfaces when two conditions are satisfied: (1) the drop must be macroscopic in size such that the curvature energy terms can be neglected and (2) the interface must remain undeformed so that deviatoric elastic stresses are not present.

If the above two conditions are met, Eqs. (7) and (8) (see Sec. III A) can be used to determine the interfacial energy of complex interfaces via the traditional shape-fitting method. The validity of the shape-fitting method can be verified by plotting the mean curvature, $1/R_s + 1/R_\phi$, as a function of the vertical height along the drop z, as proposed by Nagel *et al.* [30] [see Fig. 1(b) for a schematic of the coordinate system]. If the slope is a constant, then γ is a constant scalar.

F. Small-amplitude interfacial oscillatory shear rheology

Interfacial shear rheology experiments were conducted using a stress-controlled discovery hybrid rheometer (DHR-3) from TA Instruments equipped with a du Noüy ring and a double-wall Couette cell geometry [31], which consists of an outer glass cylinder and an internal Teflon cylinder. Low amplitude oscillatory shear experiments are conducted within the linear viscoelastic regime. The experimental protocol consists of two steps: (1) an initial amplitude sweep at a frequency of 0.1 Hz, exploring a strain range between 0.05 and 5% and (2) a 4-h time sweep at a strain of 0.3% and a frequency of 0.1 Hz. The first step is performed to ensure that the linear viscoelastic regime is being probed in all solutions. A 4-h duration for the time sweep is selected so that all moduli reach their plateau values. To minimize evaporation of the oil phase during the time sweep, the Couette cell is surrounded with a glass encasing whose top cover has a millimeter-sized gap to allow the spindle to rotate freely. Experiments are conducted with three different working solutions: 1 mg/ml asphaltene in toluene, 2.00% polymer in toluene, and 1 mg/ml asphaltene + 2.00% polymer in toluene.

G. Step-strain interfacial dilatational rheology

1. Experimental setup

Interfacial dilatational experiments are conducted using a custom-built dilatational rheometer that couples shape and pressure measurements, following the setup outlined in [30] and [32]. A schematic of the setup is provided in Fig. 1. A glass chamber (1 cm width × 0.5 cm length × 2 cm height) is filled with the desired oil solution, and a cylindrical capillary with an outer diameter of 0.8128 mm is immersed inside it. The capillary is connected to a syringe pump (Harvard Apparatus Pump 11 Elite HA110W; 100 µm Hamilton PTFE Luer Lock syringe) and a differential pressure transducer (Omega model PX164-005D5V) using PTFE tubing and a three-way T-connector. The above system is filled with DI water, taking special care to avoid the entrapment of air bubbles within the PTFE tubing that can impair the pressure measurements. The pump is used to make a pendant water drop inside the oil solution. The pendant drop profile is illuminated with a light source (CCS Inc. LAV-80SW2) and video recorded with a CCD camera (Imaging Development Systems UI-3080CP). A MATLAB script is used to extract data from the transducer using the Support Package for Arduino.

Experiments are conducted by varying the interface aging time and the compressional strain rate. The latter is controlled

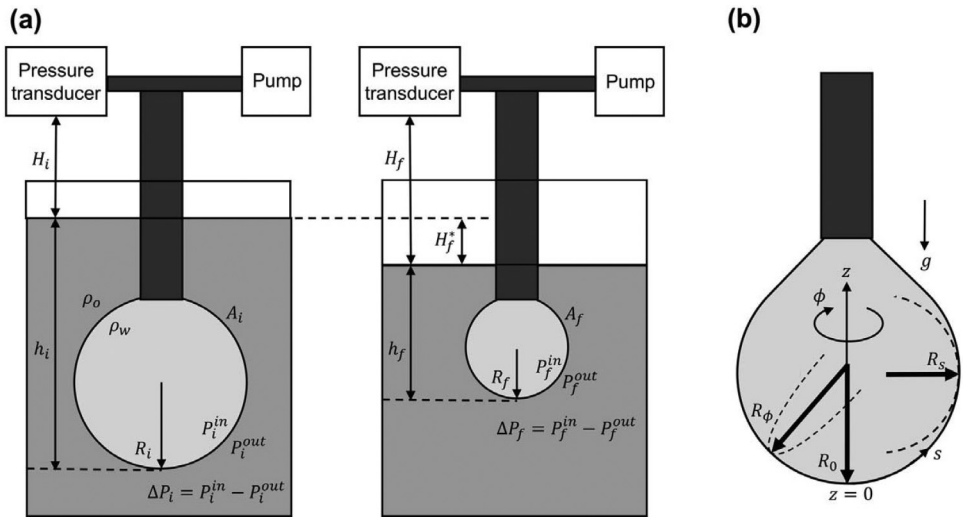

FIG. 1. (a) Schematic of the compressional step-strain experimental setup. A pendant drop of water is submerged inside an oil-filled chamber and connected to a pressure transducer and a syringe pump. (Left) 4 µl drop during the aging step. (Right) 1 µl drop during the relaxation step. The height of the oil/air interface decreases when the drop shrinks. (b) Schematic of the coordinate system used. R_s and R_ϕ are the meridional and parallel curvatures tangent to the spatial coordinates s and ϕ. The vertical axis z runs along the drop's axis of symmetry, where $z = 0$ corresponds to the drop apex.

by changing the flow rate in the syringe pump. Experiments are conducted within the nonlinear viscoelastic regime to maximize the signal-to-noise ratio in the pressure transducer output and to decrease the relative error in the drop area change calculations [30].

Each experiment consists of three steps: interface aging, strain step compression, and stress relaxation. During the first step, a water drop with a volume of 4 µl is formed at the tip of the capillary. The water drop is immersed inside the toluene solution in the glass chamber, which contains either a 1 mg/ml asphaltene or a 1 mg/ml asphaltene + 2.00% polymer-in-toluene solution. It is important to maintain a constant initial volume and surface area for all systems, since experiments are conducted within the nonlinear viscoealstic regime. This can only be achieved by working with spherical drops because the interfacial tension values are different among the two oil-water solutions. An initial drop size of 4 µl is chosen because this is the largest drop that can be formed that still remains spherical. Once the drop is formed, the top of the chamber is covered to minimize oil evaporation and the system is allowed to age for different times of 1, 10, or 60 min.

After aging is complete, a step-strain compression is applied by withdrawing fluid from the drop until a final volume of 1 µl is achieved. The compression is carried out at different flow rates of 0.01, 0.1, or 1 µl/s. Once the drop reaches its final volume, it is allowed to relax back to an equilibrium shape and pressure. A time-dependent compressional relaxation modulus is calculated during this step.

2. Data processing and modulus calculations

A time-dependent compressional relaxation modulus, $E_c(t)$, is calculated using the following expression [17,33]:

$$E_c(t) = \frac{\gamma_\mathrm{i} - \gamma_\mathrm{f}(t)}{(A_\mathrm{i} - A_\mathrm{f}(t))/A_\mathrm{i}}, \tag{1}$$

where γ_i and A_i are the interfacial energy and surface area before compression and $\gamma_\mathrm{f}(t)$ and $A_\mathrm{f}(t)$ are the time-dependent values during stress relaxation.

When the pendant water drop is deformed, stresses acting in the viscoelastic interfacial adsorption layer can become anisotropic and nonuniformly distributed throughout the drop's surface. As outlined in Sec. III A, anisotropic surface stresses can be observed with nonfluid elastic interfaces such as those seen in the asphaltene and copolymer systems studied in the present paper [30,32,34].

Since the tensorial expression for the surface energy must now be used, then two time and position-dependent compressional moduli, $E_{c,s}(t, z)$ and $E_{c,\phi}(t, z)$, are required. The full expressions for the surface energy components γ_ϕ and γ_s are provided in Sec. III A and in the Appendix. The coordinate system is depicted in Fig. 1(b).

To simplify the analysis, the spatial dependence of the modulus was removed by only calculating the modulus value at the drop apex at $z = 0$. Since the curvature at the apex is isotropic, the meridional and parallel interfacial tensions are equal and $E_{c,s}(t, z = 0) = E_{c,\phi}(t, z = 0) = E_{c,0}(t)$. The symmetry at the apex also implies that all elastic stresses are locally isotropic, rendering the interfacial energy a scalar value, as prescribed by Eq. (8). Since $R_s = R_\phi = R_0$, the normal stress balance given by Eq. (6) reduces to the Young–Laplace equation for a spherical interface, $\gamma(z = 0) = \Delta P_0 R_0/2$. Thus, the compressional relaxation modulus at the drop apex, $E_{c,0}(t)$, is now given by

$$E_{c,0}(t) = \frac{\Delta P_{0,\mathrm{i}} R_{0,\mathrm{i}} - \Delta P_{0,\mathrm{f}}(t) R_{0,\mathrm{f}}(t)}{2(A_\mathrm{i} - A_\mathrm{f}(t))/A_\mathrm{i}}. \tag{2}$$

The Laplace pressure jump at the apex ΔP_0 can be obtained from the pressure transducer by taking into account the hydrostatic pressure in the droplet and continuous phases. In Fig. 1, the subscripts "i" or "f" are used to indicate the initial (before compression) and final (during relaxation) drop

configurations,

$$\Delta P_0 = P^{\mathrm{tr}} - \rho_{\mathrm{o}} g h + \rho_{\mathrm{w}} g (h + H) - P^{\mathrm{off}}. \tag{3}$$

Here, P^{tr} is the pressure output from the transducer and P^{off} is the transducer's offset at zero pressure, which is prescribed by the manufacturer. ρ_{o} and ρ_{w} are the oil and water solution densities, respectively. As can be seen from Fig. 1, h is the vertical distance between the drop apex and the air-oil interface and H is the vertical distance between the air-oil interface and the transducer. Since H is difficult to measure accurately, Eq. (2) can be rearranged to express all quantities in terms of easily measurable variables by adding and subtracting the term $R_{0,\mathrm{f}}(t)\Delta P_{0,\mathrm{i}}$ from the numerator, as follows:

$$E_{c,0}(t) = \frac{R_{0,\mathrm{f}}(t)(\Delta P_{0,\mathrm{i}} - \Delta P_{0,\mathrm{f}}(t)) + \Delta P_{0,\mathrm{i}}(R_{0,\mathrm{i}} - R_{0,\mathrm{f}}(t))}{2(A_{\mathrm{i}} - A_{\mathrm{f}}(t))/A_{\mathrm{i}}}, \tag{4a}$$

$$\Delta P_{0,\mathrm{i}} - \Delta P_{0,\mathrm{f}}(t) = (P_{\mathrm{i}}^{\mathrm{tr}} - P_{\mathrm{f}}^{\mathrm{tr}}(t)) + (\rho_{\mathrm{w}} - \rho_{\mathrm{o}}) g (h_{\mathrm{i}} - h_{\mathrm{f}}(t)) - \rho_{\mathrm{w}} g H_{\mathrm{f}}^{*}(t), \tag{4b}$$

$$\Delta P_{0,\mathrm{i}} = 2\gamma_{\mathrm{i}}/R_{0,\mathrm{i}}. \tag{4c}$$

III. THEORY AND GOVERNING EQUATIONS

A. Surface energy of complex interfaces—The augmented Young–Laplace equation

The normal stress balance for simple interfaces is prescribed by the Young–Laplace equation, which relates the pressure jump across the interface, ΔP, to the product between the interfacial tension γ_0 and the local principal meridional and parallel curvatures, $1/R_s$ and $1/R_\phi$ [see Fig. 1(b) for a description of the coordinate system]. The pressure jump at any point along the interface can be obtained by adding the hydrostatic pressure contribution, $\Delta\rho g z$ (where $z = 0$ corresponds to the position of the drop apex) to the pressure jump at the drop's apex, ΔP_0. By taking advantage of symmetry, the pressure jump at the apex can be expressed as $\Delta P_0 = 2\gamma_0/R_0$, where R_0 is the radius at the apex [28,29],

$$\gamma_0 \left(\frac{1}{R_s} + \frac{1}{R_\phi} \right) = \Delta P \equiv \Delta P_0 \pm \Delta\rho g z \equiv \frac{2\gamma}{R_0} \pm \Delta\rho g z. \tag{5}$$

The sign of the gravitational term depends on whether the drop is buoyant or pendant.

The surface energy description presented in Eq. (5) applies to interfaces that are liquidlike in character and are unable to support a stress [29,34]. For these simple interfaces, the energy per unit area is given by a single, scalar interfacial tension. However, many interfaces are deemed "complex" due to the presence of adsorbed components that can interact with each other and allow the interface to support lateral stresses in response to straining deformations [30,32,34]. The surface energy of such complex systems is no longer given by a scalar constant and is instead replaced by two spatially varying surface stresses γ_ϕ and γ_s [30,32],

$$\left(\frac{\gamma_s}{R_s} + \frac{\gamma_\phi}{R_\phi} \right) = \Delta P_0 \pm \Delta\rho g z. \tag{6}$$

The surface stresses can depend on the Gibbs elasticity resulting from surfactant adsorption/desorption, the curvature-dependent bending and torsion energies, and interfacial viscoelasticity [30]. Expressions for γ_ϕ and γ_s are presented in the Appendix, along with a physical description of each of the terms.

In practice, many of the terms in the equation for the energy of a complex interface can be neglected. For instance, since the bending energy term scales inversely with the size of the drop, it can be shown to be negligible for macroscopic pendant drops. In addition, no deviatoric elastic stresses are incurred for static measurements where the interface shape does not change, such as the interfacial tension measurements using the pendant drop technique introduced in Sec. II E. Thus, a scalar isotropic complex surface energy can be prescribed for static macroscopic drops,

$$\gamma = \gamma_\phi = \gamma_s, \tag{7}$$

$$\gamma = \gamma_0 - \Pi_{ads}(\Gamma) + \gamma_{\mathrm{iso}}^{e}. \tag{8}$$

In the above expression, γ_0 refers to the surface tension of a clean interface, $\Pi_{\mathrm{ads}}(\Gamma)$ is the surface pressure resulting from surfactant adsorption (Gibbs elasticity), and $\gamma_{\mathrm{iso}}^{e}$ is the isotropic elastic contribution. These terms are explained in more detail in the Appendix.

Equations (6) and (7) can be used to obtain the energy per unit area of a complex, undeformed elastic interface via the pendant drop method. Equation (7) is also used for the compressional relaxation modulus calculations outlined in Sec. II G 2, since the symmetry at the drop apex renders all elastic contributions isotropic.

For microscopic drops, the bending energy contribution must be taken into account (in practice, torsion stresses are neglected [35]). The resulting expression considers the interfacial tension for a flat interface, the bending stresses associated with changes in the mean curvature, and viscoelastic stresses. Assuming that the spontaneously emulsified droplets remain spherical (i.e., $R_s = R_\phi$ and all deviatoric elastic contributions are neglected), Eq. (A1) in the Appendix for the interfacial free energy per unit area can be simplified to

$$\gamma = (\gamma_0 - \Pi_{\mathrm{ads}}(\Gamma)) - \kappa \left(\frac{2J}{R_{sc}} - \frac{J^2}{2} \right) + \gamma_{\mathrm{iso}}^{e}, \tag{9}$$

where κ is the bending modulus, J is the mean curvature, and $2/R_{sc}$ is the spontaneous curvature (which arises from the geometrical packing of the surface active species at the interface [36,37]). A more detailed explanation of these terms is provided in the Appendix.

B. Proposed mechanisms of spontaneous emulsification

1. Interfacial turbulence

Interfacial turbulence is the result of a mechanical instability of the interface caused by unsteady motions that develop when two liquid phases are brought into contact [2]. When this occurs, a localized interfacial tension gradient can instantaneously develop due to a nonuniform distribution of surfactant at the liquid-liquid interface. These gradients induce strong Marangoni stresses that, in turn, lead to violent interfacial motions [2].

For complex interfaces, the presence of a surface viscoelasticity deters the motion caused by interfacial tension gradients [33,38]. A dimensional analysis can reveal whether Marangoni stresses or viscous stresses dominate at the interface. Thus, a dimensionless Marangoni number, Ma, can be defined as the ratio of Marangoni to viscous stresses,

$$Ma = \frac{\frac{\Delta\gamma}{L}}{\frac{\eta_s^* U}{L^2}} = \frac{(\Delta\gamma)L}{\eta_s^* U} = \frac{(\Delta\gamma)\tau}{\eta_s^*}, \tag{10}$$

where $\Delta\gamma$ is the difference in surface tension between a clean and a surfactant-laden interface, η_s^* is a surface shear viscosity, U is a characteristic surface velocity, L is the length scale over which changes in surface properties occur, and τ is a time scale defined as L/U. The Marangoni stress is equal to $\Delta\gamma/L$, and the viscous stress is given by $\eta_s^* U/L^2$. If $Ma \gg 1$, Marangoni flows dominate the interfacial dynamics and emulsion formation is driven by turbulent surface motions. Otherwise, if $Ma \ll 1$, the presence of an interfacial viscosity prevents the onset of interfacial turbulence.

2. Diffusion and stranding

Spontaneous emulsification can also occur whenever the diffusion of the solvent into an immiscible phase creates regions of local supersaturation, which can nucleate and develop into droplets [1]. Thus, this mechanism is a chemical rather than a mechanical phenomenon and is, therefore, independent of the magnitude of the interfacial tension [2]; however, it requires the presence of a solute in one of the phases, which can be surface active or not. Diffusion and stranding was first postulated by Davis and Rideal [16] in 1961. The analysis was later extended by Ruschak and Miller [8], who solved the time-dependent 1D diffusion equation with a moving boundary to derive concentration profiles for the solute and solvents [8]. Because a similarity solution exists, the diffusion paths of all three components (both solvents and the solute) can be plotted in a single ternary phase diagram, which reveals the existence of a locally supersaturated region where emulsification is expected to occur [8].

More recently, it has been reported in the literature that the diffusion and stranding mechanism is sensitive to the osmotic pressure jump across the interface [10,39]. Duboué *et al.* reported the spontaneous formation of a water-in-oil emulsion in a system composed of asphaltenes dissolved in toluene and water [10]. They propose a mechanism whereby molecular water diffuses into the toluene phase, where it encounters and binds to the polar sites of the asphaltene aggregates. Since asphaltenes are surface active, their concentration at and near the interface is significantly higher than in the bulk oil phase, facilitating the encounter of a water molecule and an asphaltene cluster. Subsequently, the hydrated asphaltenes aggregate with each other and a "nucleus," or a very small droplet, is formed. This droplet continues increasing in size from further diffusion of molecular water.

The growth rate of the droplets is controlled by the osmotic pressure difference resulting from the change in chemical potential between the bulk and the solubilized water. For example, if the osmotic pressure in the bulk water phase is decreased through the addition of salt, spontaneous emulsification is suppressed [10]. This effect has also been reported in solutions of crude oil and brine [39] and in aqueous polymeric systems [40].

3. Interfacial bending

The free energy of simple interfaces is minimized when the total interfacial area is minimized or when the two phases are entirely separated. However, in certain systems where the interfacial tension is near zero but still positive, the interface can become thermodynamically unstable with respect to bending motions and subsequently break up [41–43]. Thus, spontaneous emulsification is due to a thermodynamic instability with respect to a change in interfacial mean curvature, where the net change in interfacial free energy resulting from bending stresses is enough to offset the energy penalty associated with an increase in the surface area [42].

The model prescribed by Eq. (9) (ignoring elastic contributions) was first postulated by Helfrich in the context of lipid bilayers with vanishing interfacial tensions [44] and later augmented by Murphy [42], de Gennes and Taupin [35], and others [45–47]. Emulsion formation is favored when R_{sc} is lowered and κ is increased [48]. Typical values of κ have been measured to be between 0.1 and 100 k_BT (where k_B is the Boltzmann constant) [37,46,49]. For a system where $(\gamma_0 - \Pi_{ads}(\Gamma)) \lesssim 1\ \mathrm{mN/m}$ and $10 < R_{sc} < 1000\ \mathrm{nm}$, spontaneous emulsification is energetically favorable [50]. In practice, a spontaneous curvature can be attained through the use of surfactants with an asymmetric distribution of hydrophobic and hydrophilic domains or through the addition of a cosurfactant that increases the heterogeneity of the interface [48].

As mentioned in Sec. II A, upon adsorption to a toluene-water interface, the bulk of an asphaltene aggregate will be located in the oil phase. This favors the existence of a spontaneous curvature that bends the interface away from the oil phase and could potentially explain the formation of a water-in-oil emulsion.

IV. RESULTS

A. Use of polymeric flow improvers to control the rate and extent of spontaneous emulsification

Brightfield microscopy experiments were carried out using different asphaltene-polymer mixtures, as outlined in Sec. II B. Representative snapshots of the interface at

different asphaltene and polymer concentrations (columns) and time points (rows) are shown in Fig. 2. The leftmost column presents the temporal evolution of an asphaltene-only solution. Droplet formation begins shortly after the phases are contacted. Droplets with an average size of around 10 μm gather at the interface and laterally migrate toward the bottom of the meniscus region (at the center of the photograph). After 10 min, the droplet density has increased to almost completely cover the interface, forming a dense monolayer. After 60 min, multiple layers of spontaneously emulsified droplets continue to gather and accumulate at the interface. These multiple layers can be visualized by slowly moving the objective in the vertical direction. The image reveals the existence of some larger drops ($\sim$ 50 μm in size), which form as a result of coalescence events that occur when the droplet density is high.

Emulsification is largely suppressed when the polymer is added to the asphaltene-in-toluene solution. A slight reduction in the number and size of emulsified droplets is seen when 0.25% of the polymer is added (second column in Fig. 2). For instance, after 60 min, only one monolayer of droplets is visible at the interface. When the polymer concentration is increased to 2.00% (third column), emulsion formation is almost entirely suppressed and only a few small ($\lesssim$5 μm) droplets are scattered at the interface. The same effect was seen at higher copolymer concentrations. Experiments in the absence of asphaltene were also performed using a 2.00% polymer-in-toluene solution (rightmost column). The images show that the polymer by itself can also induce spontaneous emulsification, albeit to a much lesser extent than asphaltenes. Although the droplet morphology and spatial distribution is different with 2.00% polymer in the presence and absence of asphaltenes (the droplets are less smooth and more homogeneously distributed when asphaltenes are present), the average droplet size and concentration is comparable in both cases.

The rate and extent of spontaneous emulsification can be further quantified by tracking the time evolution of the size and number of droplets. A "normalized emulsified area," or NEA, is defined as the sum of the projected areas of all droplets of a given size, divided by the surface area of the image. Similarly, the "total normalized emulsified area," or total NEA, is given by the sum of the projected area of *all* droplets normalized by the image surface area.

Figure 3 shows plots of the total NEA (left pane) and the NEA as a function of particle radius at different times (right pane) for all asphaltene-polymer compositions used. The total NEA decreases as the concentration of polymer increases. The total NEA for the asphaltene-only solution, shown in red, continuously increases with time, indicating

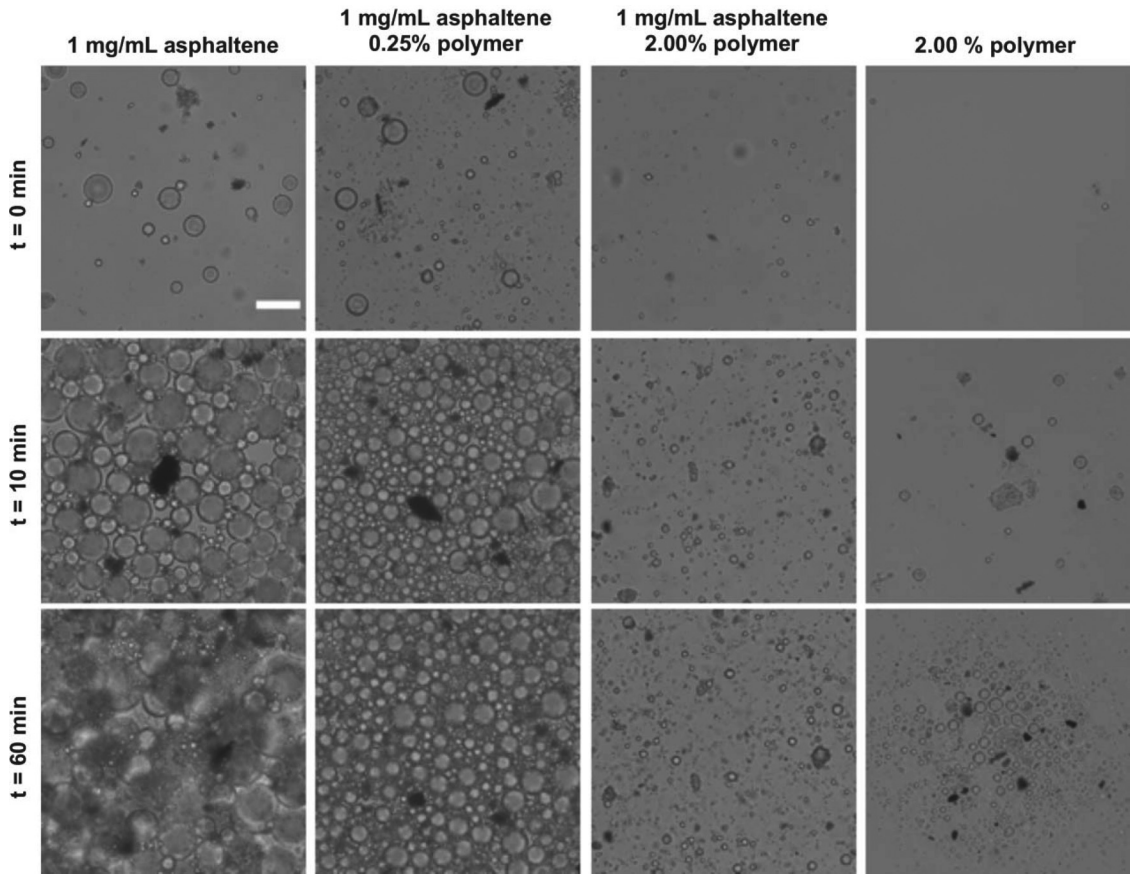

FIG. 2. Spontaneous emulsification as a function of time for different asphaltene and polymer concentrations (scale bar = 50 μm). The water phase consists of DI water and the oil phase is composed of toluene, asphaltene, and/or polymer. Each column represents a different asphaltene and polymer concentration. Top row: immediately upon contact of water and oil phases. Middle row: 10 min after contact of water and oil phases. Bottom row: 60 min after contact of water and oil phases. Both pure asphaltene and pure polymer systems spontaneously emulsify. In the presence of asphaltenes, the higher the copolymer concentration, the lower the degree of emulsion formation.

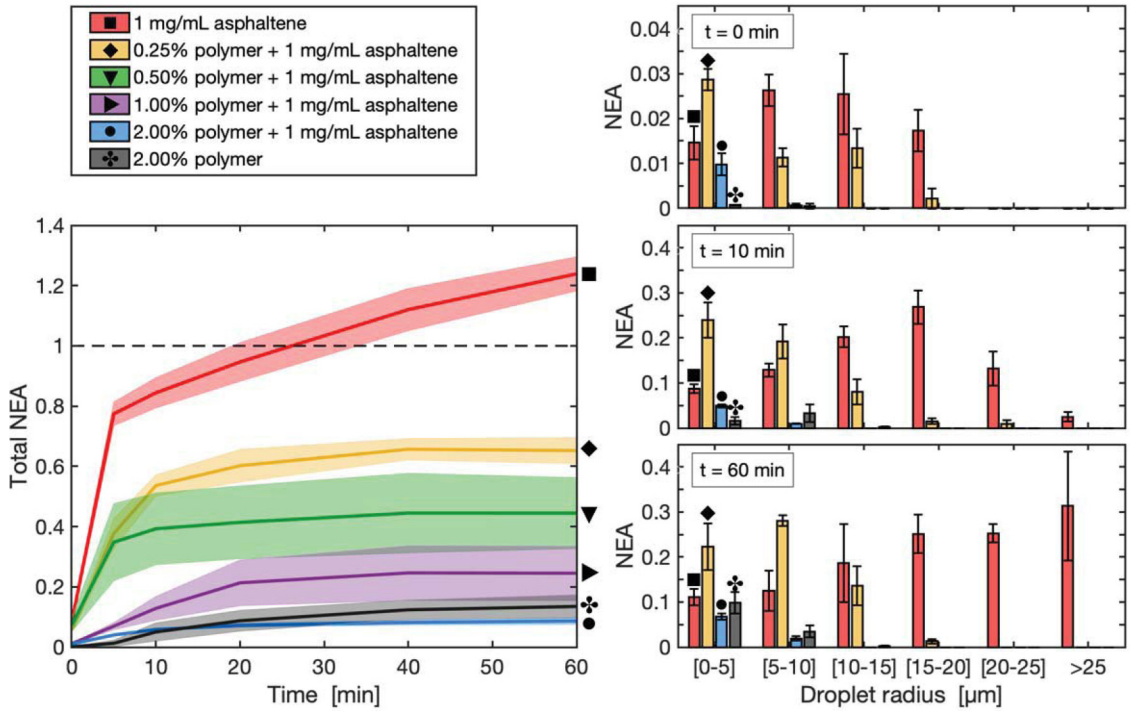

FIG. 3. (Left) Total normalized emulsified area (NEA) as a function of time for different asphaltene and polymer concentrations. The higher the polymer concentration, the lower the emulsified area. The horizontal dotted line at a total NEA of 1 represents a full monolayer coverage of the interface by emulsified droplets. For systems where the total NEA is larger than 1, multiple layers of droplets are present. (Right) Droplet area distribution at 0 min (top), 10 min (middle), and 60 min (bottom) for different asphaltene and polymer concentrations.

that an emulsion keeps forming well beyond the 1 h observation window. After approximately 25 min, the total NEA increases beyond unity, indicating that multiple layers of spontaneously emulsified droplets are present at the interface. In contrast, the curves corresponding to polymer-laden solutions eventually plateau, showing that emulsifiation is arrested within a 30 min window after the aqueous and oil phases have been contacted.

Plots of the NEA as a function of the droplet radius show how the distribution of droplet sizes evolves as a function of time. At early times ($t = 0$ min), the average droplet size shifts toward smaller radii with increasing copolymer concentration. As time proceeds ($t = 10$ min, note the change in y axis scale) the number of small droplets (those with radii between 0 and 10 μm) increases for all systems, showing continuous emulsion formation. The mean droplet radius for the asphaltene-only system increases because the interface is approximately 80% covered in droplets, increasing the frequency of coalescence events. Coalescence events and diffusion of molecular water continue to occur, shifting the mean droplet radius further to the right. After 60 min, the average droplet size for the 1 mg/ml asphaltene + 0.25% polymer solution also shifts toward larger droplets, again due to the combined effect of diffusion and drop-drop coalescence.

We have shown that the presence of a polymeric flow improver, (*alt*)SNODMI, is capable of dramatically reducing the rate and extent of spontaneous emulsion formation in the presence of asphaltenes. It is important to note that this polymer is also able to induce spontaneous emulsification, although to a lesser extent than asphaltenes. Sections IV B and IV C aim to elucidate the mechanism behind how spontaneous emulsification in the presence of asphaltenes proceeds, and how rheological properties at the fluid-fluid interface are correlated to the extent of emulsion formation.

B. Mechanism of spontaneous emulsification in the presence of asphaltene adsorption

1. Interfacial energy measurements

Figure 4 presents a plot of the interfacial tension as a function of time for all asphaltene-polymer systems studied. The interfacial energy per unit area was measured for millimeter-sized drops using the pendant drop method. The surface tension of a pure toluene-water system is shown by the dotted line and is constant at 36 mN/m.

When asphaltenes are added to the toluene phase, they adsorb at the toluene-water interface and lower the interfacial energy. As seen in the supplemental material [54], the curvature profile with respect to the height along the drop for asphaltene-laden toluene-water interfaces is indeed linear at short times, confirming the validity of Eqs. (6) and (7). Over time, slight changes in the pendant drop profile occur as the interfacial energy decreases. However, since the deformations in the drop shape are quasistatic, the deviatoric elastic stress contribution to the surface energy is negligible and the Young–Laplace equation for an isotropic interfacial tension still remains valid. This is once again verified through the linear relation between the curvature profile and the height along the drop.

In order for the interfacial turbulence hypothesis to be valid, the surface tension gradient must be sufficiently large to induce Marangoni stresses that are not dampened by

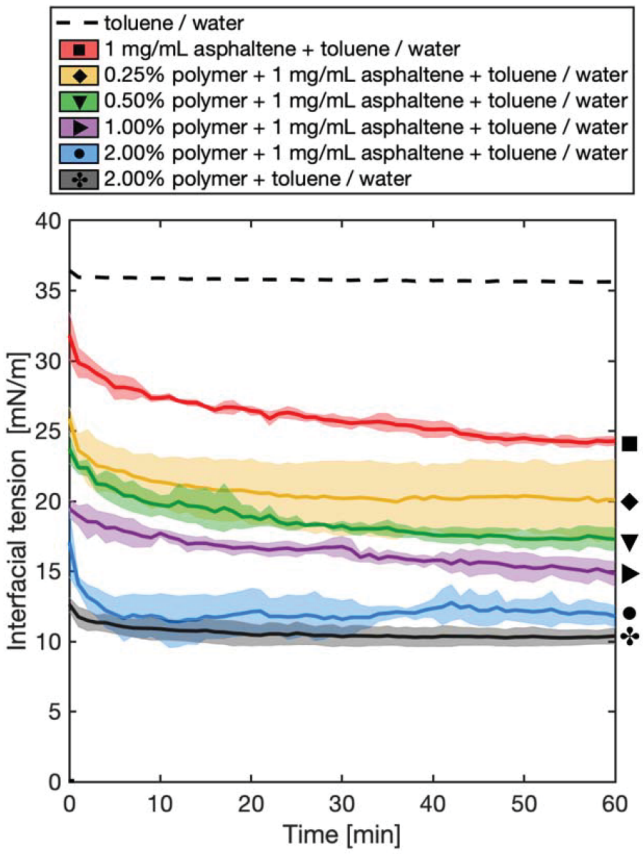

FIG. 4. Interfacial tension measured using the pendant drop method for different asphaltene and polymer concentrations as a function of time. The interfacial tension decreases as the polymer concentration increases, showing that polymer competitively adsorbs onto the oil/water interface and lowers the surface energy.

viscous dissipation at the interface [i.e., the magnitude of the surface Marangoni number *Ma* must be greater than or equal to unity, as defined in Eq. (10)]. The magnitude of *Ma* can be calculated by taking the ratio of the surface tension difference, $\Delta\gamma$, divided by a viscous energy dissipation term η_s^*/τ, where η_s^* is a surface viscosity and τ is a characteristic time scale.

As shown in Fig. 4, the difference in the interfacial tension values for a pure toluene-water and an asphaltene-toluene-water system is approximately equal to 10 mN/m. We take η_s^* to be the complex interfacial shear viscosity, defined as follows [51,52]:

$$\eta_s^* = iG^*/\omega = (G'' - iG')/\omega, \tag{11}$$

where i is the unit imaginary number, ω is the rheometer oscillation frequency, and G'' and G' are the interfacial shear viscous and elastic moduli, which are themselves functions of ω. The magnitude of η_s^* is defined as the absolute value of the complex surface viscosity [51]

$$|\eta_s^*| = \sqrt{G'^2 + G''^2}/\omega. \tag{12}$$

As outlined in Sec. II F, small-amplitude interfacial oscillatory shear rheology experiments were conducted in order to extract the linear viscoelastic behavior of the interface when subject to shear deformations. The data are shown in Fig. 6, and a discussion of the experimental results is provided in Sec. IV C 1. For a pure asphaltene solution, η_s^* is approximately equal to 30 mN/m s at early times ($t \simeq 0$) and 120 mN/m s at as $t \to \infty$. Finally, we define a characteristic time τ as the time it takes for an emulsion to start to form, which is on the order of seconds. According to Eq. (10), $0.08 \lesssim Ma \lesssim 0.33$, suggesting that surface viscoelastic stresses impede turbulent motions at the interface. Thus, the interfacial turbulence mechanism is not responsible for the formation of a stable water-in-oil emulsion.

Furthermore, the interfacial energy per unit area for asphaltene-laden toluene-water interfaces is not vanishingly small as required by the interfacial bending hypothesis. Moreover, as increasing concentrations of the polymer are added to the asphaltene-toluene solution the interfacial tension decreases further, revealing that polymer competitively adsorbs onto the oil/water interface and displaces the adsorbed asphaltenes. Although the interfacial tension decreases to around 10 mN/m for 2.00% copolymer systems, this value is also not vanishingly small.

The results of Fig. 4 raise concerns regarding the validity of the interfacial bending hypothesis. As mentioned previously, the interfacial tension of none of the systems studied is vanishingly small. Furthermore, the fact that systems with higher copolymer contents have a lower surface energy than a pure asphaltene-in-toluene solution, which contradicts the fact that the asphaltene-only systems emulsify to larger extents. Although these results point to the fact that the tendency of asphaltene-laden systems to spontaneously emulsify is not correlated to their interfacial tension values, it is important to note that the results of Fig. 4 are applicable only to macroscopic interfaces where bending stresses are neglected and may not adequately represent the interfacial energy per unit area of a highly curved interface (i.e., a spontaneously emulsified droplet). Section IV B 2 outlines further experiments that were conducted using fluorescence microscopy. These experiments are aimed to better understand the transport dynamics at the oil-water interface and assess the validity of the interfacial bending hypothesis.

2. *Fluorescence microscopy studies*

The results from the fluorescence confocal experiments for a spontaneously emulsified asphaltene system are presented in Fig. 5. The brightfield images are shown on the leftmost column, where the spontaneously emulsified droplets are clearly visible. The rightmost column shows the fluorescence signal when the oil-soluble fluorophore BDP is excited; thus, the oil phase is indicated through the presence of the fluorophore. Similarly, the center column presents the fluorescent signal when the aqueous dye SC5.5 is excited. In this panel, the fluorophore is present in the aqueous phase. Each row corresponds to a different z-position in the stack; from top to bottom, the focal plane moves vertically upward.

The water droplets seen in the brightfield images can also be identified as black, nonfluoresceing circles in the BDP signal. However, the same emulsified droplets cannot be seen in the SC5.5 signal, indicating that the aqueous

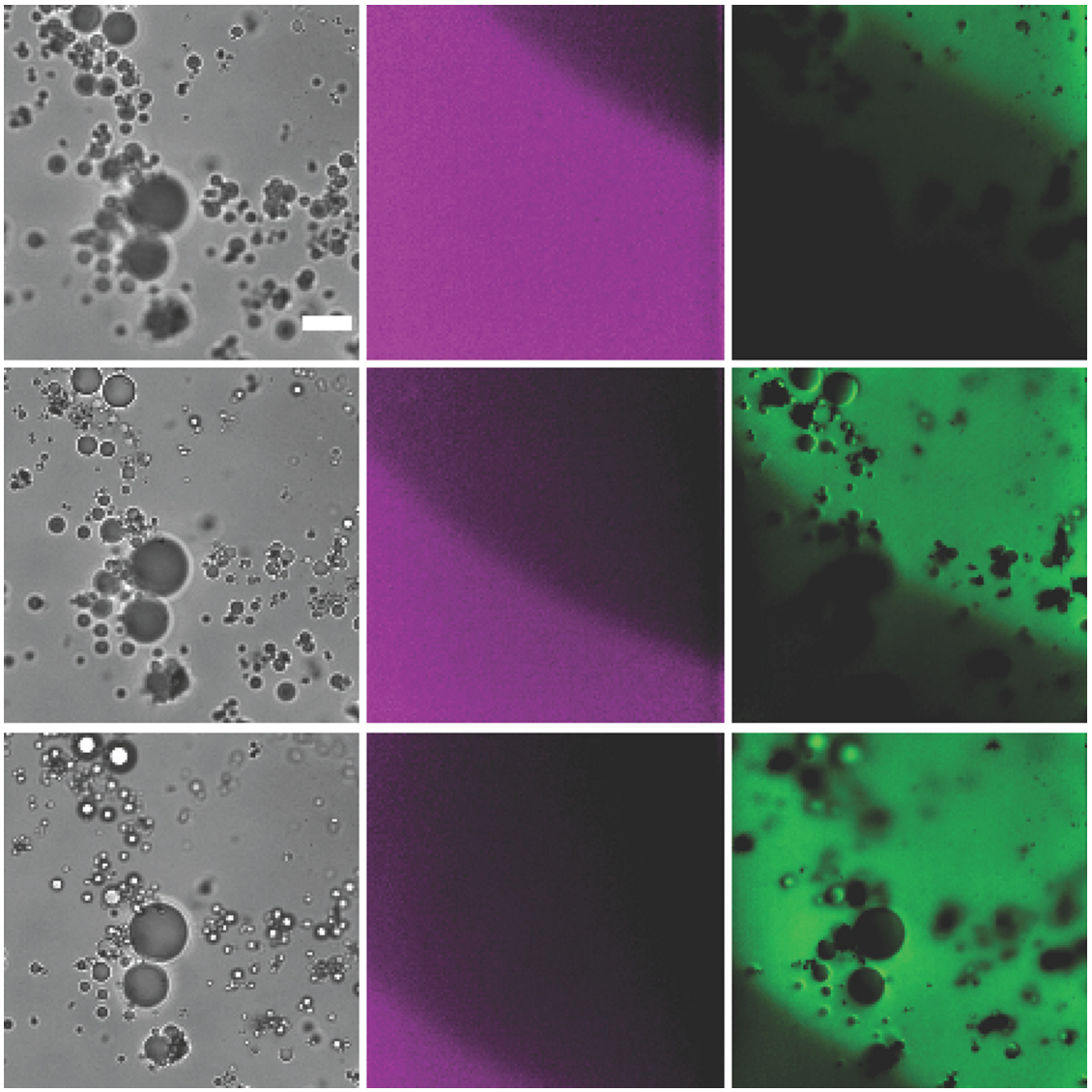

FIG. 5. Brightfield and fluorescence images of the interface between water and an asphaltene-in-toluene solution, taken using a confocal microscope (scale bar = 20 μm). Aqueous phase: 6 ng/ml sulfocyanine 5.5 in DI water. Oil phase: 0.25 mg/ml asphaltene and 75 ng/ml BDP FL azide in toluene. Left panel: brightfield signal, center panel: aqueous fluorescence signal, and right panel: oleic fluorescence signal. Each row represents a different height along the water-oil interface; from top to bottom, the focal plane moves vertically upward from the water phase into the oil phase.

fluorophore is not carried into the droplets during emulsion formation. These results suggest that spontaneous emulsification in the presence of asphaltenes occurs via diffusion of molecular water into the oil phase and subsequent aggregation of the water and asphaltene moieties, as proposed by Duboué *et al*. It is reasonable to assume that if an interfacial bending mechanism was responsible for spontaneous emulsification, both water and SC5.5 molecules would be swept into the emulsified droplet as the interface bends.

3. SAXS measurements

The scattering intensity $I(q)$ is obtained as a function of the wavevector q for a 1 mg/ml asphaltene-in-toluene solution and a 1 mg/ml asphaltene + 2.00% polymer-in-toluene solution, as outlined in Sec. II D. The data were fit to a Guinier–Porod unified model to determine the radius of gyration of the aggregate. Apparent radii of gyration of 1.55 ± 0.05 and 1.77 ± 0.07 nm are obtained for the 1 mg/ml asphaltene solution and the 1 mg/ml asphaltene + 2.00% polymer solution, respectively. Similar sizes for asphaltene aggregates are reported in the literature [19,20].

The larger size of the asphaltene + polymer structures suggests that the polymer is forming complexes with the dissolved asphaltenes in solution. Sections IV B 1 and IV B 2 showed that spontaneous emulsification of asphaltene-laden solutions occurs via the diffusion of molecular water into the bulk oil phase and their subsequent binding with the asphaltene aggregates. Thus, it hypothesized that the polymer reduces the access of molecular water to the polar moieties of the asphaltenes, either by directly binding with them or by making them sterically inaccessible. This prevents some water molecules from binding with the dissolved asphaltenes and nucleating into spontaneously emulsified drops.

A fraction of the polymer remains in solution, where it binds to the dissolved asphaltenes, and a fraction of the

polymer migrates and adsorbs onto the oil/water interface. Thus, the polymer competes with water for access to the asphaltenes and also with the asphaltenes for access to the interface.

C. The role of interfacial viscoelasticity in spontaneous emulsification

Section III B outlined different mechanisms that could be responsible for the spontaneous emulsification of asphaltene-laden solutions. It was established that a diffusion and stranding process occurs, whereby diffusion of molecular water across the interface and subsequent binding with asphaltene aggregates gives rise to an emulsion of micrometer-sized drops. Although diffusion and stranding is the result of a gradient in chemical potential and is independent of the surface energy of the interface, it is known that interfacial viscoelasticity affects the rate of spontaneous emulsification in asphaltene-laden solutions [13].

This section aims to further elucidate how interfacial viscoelasticity is correlated to the rate of spontaneous emulsification in asphaltene-laden water-toluene systems. Since polymer competitively adsorbs onto toluene-water interfaces and lowers the surface energy, its presence could also affect the viscoelastic properties of the interface. The latter could potentially be correlated to the tendency of the systems under study to spontaneously emulsify. Both interfacial oscillatory shear and step-strain dilatational rheological experiments were performed in order to examine the interfaces' response to various modes of deformation.

1. Interfacial oscillatory shear rheology

Figure 6 plots the results of the interfacial shear time sweep experiments (data for the amplitude sweep are presented in the supplementary material [54]). Three different oil phase compositions were studied: 1 mg/ml asphaltene, 1 mg/ml asphaltene + 2.00% polymer, and 2.00% polymer. The solid lines represent the elastic or storage modulus and the dotted lines show the viscous modulus. All interfaces show an elastic-dominated response.

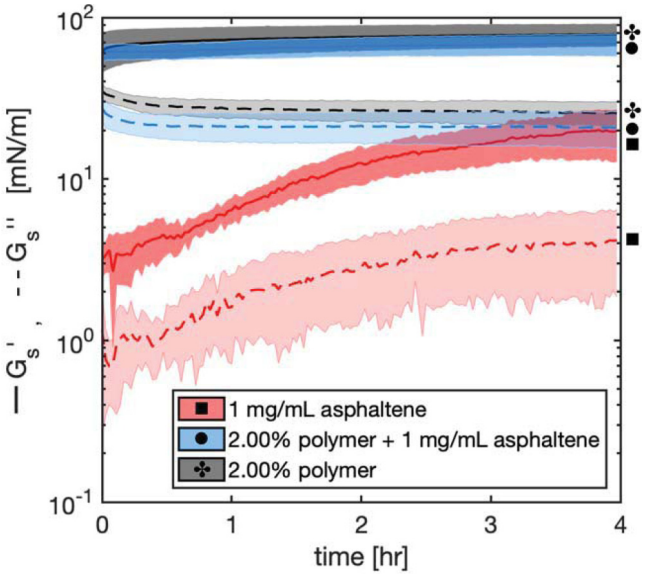

FIG. 6. Small-amplitude oscillatory interfacial shear rheology of different asphaltene and polymer mixtures as a function of time for a strain of 0.3% and a frequency of 0.1 Hz within the linear viscoelastic regime. The solid lines represent the elastic modulus, and the dotted lines represent the viscous modulus.

The stress-strain response is almost identical for polymer-laden interfaces in the presence or absence of asphaltenes, in agreement with Fig. 4, which shows analogous values for the interfacial energy. These interfaces also exhibit constant moduli over time, which is evidence of fast adsorption and a rapid formation of an interfacial microstructure. This indicates that in the case of mixed polymer and asphaltene adsorption, large asphaltene clusters either do not have sufficient time to reach to the interface (a diffusion argument) or they are being quickly displaced by the copolymer (a kinetic argument).

The elastic and viscous moduli for the polymer-laden systems are initially more than an order of magnitude higher than those of the 1 mg/ml asphaltene solution. In the latter case, the moduli increase over time for approximately 2.5 h, depicting the gradual formation of an interfacial microstructure that is accompanied by a decrease in the interfacial energy, as shown in Fig. 4.

2. Interfacial dilatational step-strain rheology

Typical results for the drop surface area A_f, apical pressure jump $\Delta P_{0,f}$, and compressional relaxation modulus $E_{c,0}$ are shown in Fig. 7 for an aging time of 60 min and a compressional rate of $0.1\,\mu l/s$. A_f is calculated assuming the drop surface is smooth and axisymmetric. The asphaltene-only system is shown on the left and the asphaltene and copolymer solution is depicted on the right. Snapshots of the drop profile during the relaxation process are shown below each plot at times of 0, 100, and 200 s after the relaxation process has begun.

Asphaltene-only drops remain spherical during the relaxation process, as seen from the snapshots and the constant equilibrium value for the surface area. The snapshots also reveal the existence of emulsified droplets that cling to the bottom of the oil/water interface. Even though there is no macroscopic shape change, the relaxation process is accompanied by a microstructural rearrangement and reconfiguration at the interface, as evidenced through the pressure relaxation. This increase in the internal pressure of the drop translates to a decrease in its compressional relaxation modulus down to a plateau value.

When the copolymer is added to the asphaltene solution, a more complex relaxation behavior is observed. As the elastic polymer-laden drop is compressed it exhibits a significant resistance to deformation. The yielding of the drop shape first appears in the vicinity of the neck of the capillary, where it experiences the highest shear rate magnitudes. This is accompanied by the appearance of wrinkles along the vertical axis, which can be observed in the snapshot corresponding to $t = 0$ s. These wrinkles are short-lived and disappear as the drop relaxes back to an equilibrium spherical shape. During the relaxation process the neck of the drop shrinks

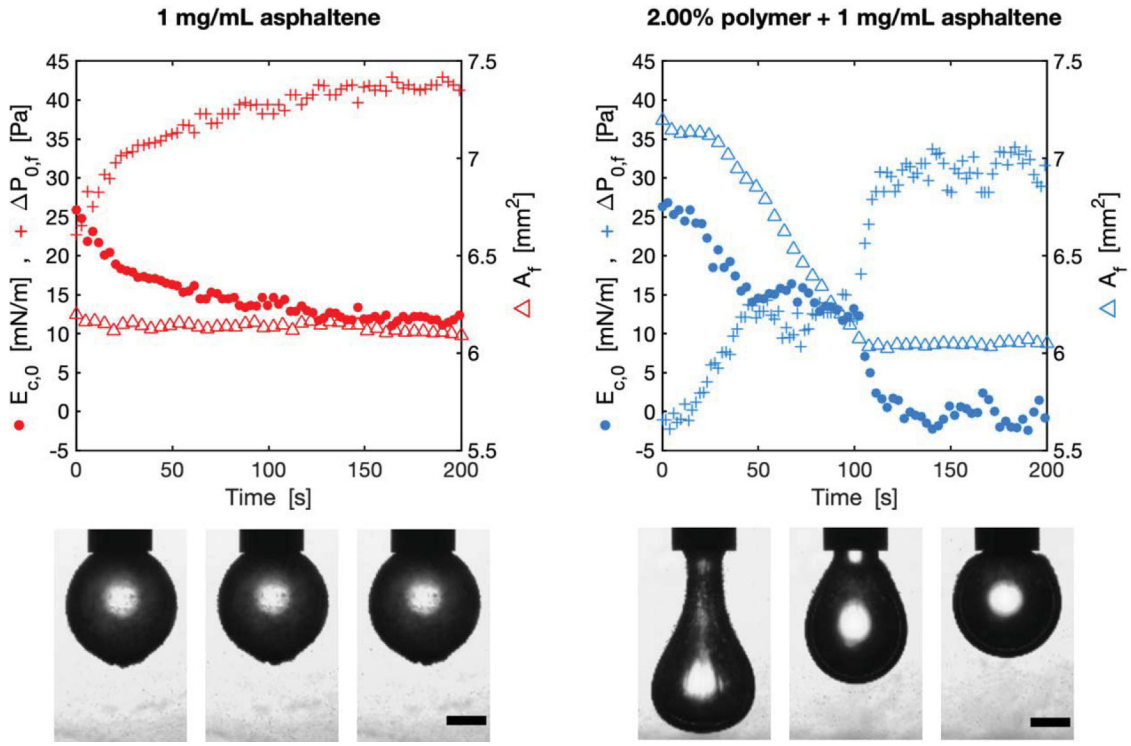

FIG. 7. Compressional step-strain relaxation profiles for 1 mg/ml asphaltene (left) and 1 mg/ml asphaltene + 2.00% polymer (right) oil solutions at an aging time of 60 min and a compressional rate of 0.1 μl/s. Snapshots are shown at times 0, 100, and 200 s after stress relaxation begins (scale bar = 0.5 mm). Asphaltene-only interfaces show a time-dependent pressure relaxation behavior but no shape change upon compression. For the same aging time and flow rate, the polymer-laden system shows both a shape and a pressure relaxation.

until it disappears. Graphically this is depicted by a quasilinear decrease in the surface area and a concomitant increase in the pressure. A negative pressure jump is observed at early relaxation times. This occurs because the elastic interface resists compressional deformations that reduce the total surface area. The anisotropic elastic terms [$\gamma^e_\phi - \gamma^e_{\rm iso}$ and $\gamma^e_s - \gamma^e_{\rm iso}$ in Eq. (A1)] significantly contribute to the surface energy of the relaxing polymer drop.

Different shape and pressure relaxation behaviors are obtained by varying the aging time and strain rate of the interface. A summary of these results is shown in Fig. 8 for the same 1 mg/ml asphaltene (left) and the 2.00% polymer + 1 mg/ml asphaltene (right) systems. Aging time is plotted on the x axis and the flow rates are shown as different shades of the same color. The top row shows the change in surface area during relaxation, $A_f^{t\to\infty}/A_f^{t=0}$. There is an absence of a macroscopic shape relaxation for asphaltene solutions and a predominant flow rate dependence for the 2.00% polymer + asphaltene system.

The initial compressional relaxation modulus $E_{c,0}^{t=0} = E_c(t=0)$ is shown in the middle row. $E_{c,0}^{t=0}$ represents the accumulation of elastic energy during compression and is on average larger in the presence of the 2.00% polymer. For the asphaltene-only interface, $E_{c,0}^{t=0}$ is an increasing function of both aging time and flow rate. The dependence on aging time shows that a viscoelastic network gradually forms at the interface, a trend which was also present in the shear experiments in Sec. IV C 1. The dependence on flow rate is indicative of the competition between the strain deformation and the interfacial rearrangement time scales. Conversely, $E_{c,0}^{t=0}$ is only a function of flow rate for the polymer-laden interface. The weak dependence on aging time suggests that a viscoelastic network forms rapidly in the presence of the polymer, a result that is also consistent with the data presented in Fig. 6.

Once deformed, the strained interfacial network will relax the imposed stress via macro- and microscopic surface rearrangements. The static compressional relaxation modulus, $E_{c,0}^{t\to\infty} = E_c(t\to\infty)$, is the long-time equilibrium value of the surface elastic energy and is shown on the bottom row of Fig. 8. Physically, $E_{c,0}^{t\to\infty}$ represents the degree of irreversibility of the film or its solidlike character [33]. Interestingly, although the polymer-containing interfaces initially resist deformation more than the asphaltene-only system, they are also better able to dissipate the accumulated elastic energy. $E_{c,0}^{t\to\infty}$ is zero for all polymer systems, which means that the initial (undeformed) and final interfacial energy of these interfaces is identical. This renders these viscoelastic liquid interfaces fully reversible.

On the other hand, $E_{c,0}^{t\to\infty}$ is finite for the asphaltene-only interfaces and increases with aging time. These results show that over time asphaltenes irreversibly adsorb onto a toluene-water interface, forming a highly solid interface that gives asphaltene-laden emulsions their long-term stability. These results agree with those presented in the study conducted by Freer and Radke, who measured the compressional moduli of asphaltene-toluene solutions in contact with water after 24 h of aging [17]. Although their experiments were conducted at low strains within the linear viscoelastic regime and the interfacial tension values were calculated using shape fitting (and

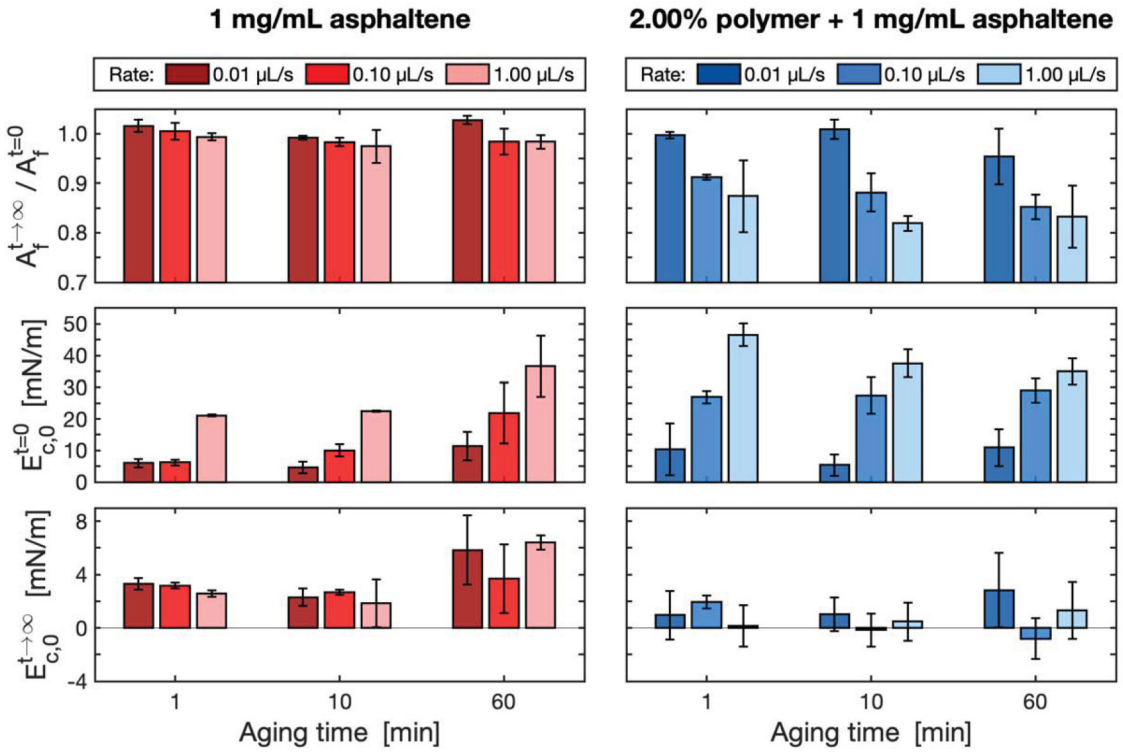

FIG. 8. Compressional step-strain experiments for 1 mg/ml asphaltene (left) and 1 mg/ml asphaltene + 2.00% polymer (right). Experiments are performed by varying the interface aging time (1, 10, and 60 min) and the compression flow rate (0.01, 0.1, and 1 µl/s). Top row: change in surface area during relaxation, $A_f^{t\to\infty}/A_f^{t=0}$. Middle row: initial compressional relaxation modulus, $E_{c,0}^{t=0}$. Bottom row: equilibrium compressional relaxation modulus, $E_{c,0}^{t\to\infty}$.

no pressure data), their initial and static moduli values are of comparable magnitude as those reported in this study. Moreover, they showed that even after repeatedly washing out the bulk oil phase with pure toluene, the interfacial tension and stress-relaxation behavior did not appreciably change, indicating that most asphaltene aggregates are irreversibly adsorbed onto the toluene-water interface [17]. Analogous results were also seen with crude oil systems containing asphaltenes [53].

Data for Figs. 7 and 8 were obtained using Eq. (4). To check the validity of this expression, $E_{c,0}(t)$ was also calculated using the CMD method originally proposed by Danov *et al.* to obtain the interfacial tension of anisotropic interfaces [32]. The open source MATLAB software developed by Nagel *et al.* was used to calculate the anisotropic interfacial stresses γ_s and γ_ϕ [30]. Then, the values at the drop apex were used to calculate $E_{c,0}$. Sample outputs for γ_s, γ_ϕ, and $E_{c,0}$ for a 1 mg/ml asphaltene and a 1 mg/ml asphalten + 2.00% polymer system are presented in the supplementary material [54].

V. DISCUSSION

When asphaltenes adsorb onto a toluene-water interface, they lead to the spontaneous formation of a water-in-oil emulsion that minimizes the total system free energy. This phenomenon is driven by gradients in chemical potential across the bulk phases, which cause molecular water to diffuse across the interface and bind to the polar sites of asphaltene aggregates. The presence of the polymeric flow improvers in the oil phase, such as (*alt*)SNODMI, can hinder (but not totally eliminate) the spontaneous emulsification phenomenon. On one hand, SAXS measurements reveal that the polymer can bind to dissolved asphaltenes and forms complexes in the bulk oil phase. In this way, dissolved polymer may hinder the ability of molecular water that has diffused into the oil phase to bind to the polar sites of the asphaltene aggregates, preventing the nucleation of new emulsified droplets. On the other hand, it is known that the copolymers competitively adsorb onto the toluene-water interface and lower the surface energy. Moreover, they quickly form stable microscopic networks that render the interface highly viscoelastic. In contrast, asphaltenes exhibit lower moduli magnitudes and a gradual buildup of interfacial viscoelasticity. It is believed that interfacial viscoelasticity also influences the rate and extent of spontaneous emulsification.

The shear and dilatational studies for asphaltene-laden surfaces in the presence and absence of the polymer reveal how each interface responds to different modes of deformation. For a 1 mg/ml asphaltene solution, both oscillatory shear and compressional step-strain experiments show that the formation of a solidlike viscoelastic network is a time-dependent phenomenon. The resistance to area-changing dilatational deformations is stronger than the resistance to shear deformations. For instance, after 60 min of aging, the initial compressional relaxation modulus is almost an order of magnitude higher than the shear elastic and viscous moduli. Since asphaltenes irreversibly adsorb onto toluene-water interfaces, the resistance to area-changing deformations is expected to be larger than the resistance to shear deformations.

When the (*alt*)SNODMI polymer is added to the asphaltene solution, the shear moduli are higher than the compressional moduli. The strain-stress response is time independent, indicating that a solidlike interfacial microstructure forms quickly. This interfacial network exhibits high resistance to shear and compressional deformations but can relax back to its initial configuration, showing that polymer adsorption is reversible.

Several parallels can be drawn by comparing the trends in interfacial viscoelasticity seen in Figs. 6 and 8 with the spontaneous emulsification behavior in Fig. 3. Systems that emulsify the least (i.e those that contain higher fractions of the polymer) also have the highest shear and dilatational moduli. For example, consider the 1 mg/ml asphaltene + 2.00% polymer system depicted in blue in all figures. The slope and magnitude of the total NEA in Fig. 3 are low, indicative of a slow rate and extent of emulsion formation. On the other hand, asphaltene-only surfaces exhibit a time-dependent behavior—as the interface becomes more viscoelastic, the rate of emulsification also decreases as evidenced from the decreasing slope of the total NEA. Thus, interfacial shear and dilatational viscoelasticity is inversely correlated to the propensity of a system to spontaneously emulsify.

These results show that the presence of interfacial viscoelasticity can be both directly and inversely correlated to emulsion stability. Depending on whether the emulsion is mechanically or spontaneously generated, the presence of interfacial viscoelasticity can either enhance or hinder emulsification. If an emulsion is mechanically generated by supplying an external energy input, the presence of an elastic interface will stabilize the mechanically emulsified droplets by forming a rigid interfacial network that inhibits coalescence [4]. On the other hand, as has been shown in the present study for spontaneously emulsified systems, the rapid formation of an elastic interfacial microstructure is correlated to slower rates of emulsion formation. It is hypothesized that the presence of a highly dense surface network acts to suppress spontaneous emulsification in two different ways: (1) mechanically, by acting as a semipermeable membrane that decreases the rate of molecular diffusion across the interface and (2) chemically, by changing the interfacial energy and subsequently the osmotic pressure which drives molecular transport across the interface. A study of the effects of interfacial viscoelasticity on the transinterfacial diffusion of small molecules is a logical direction for future works.

The aforementioned results, therefore, suggest that interfacial viscoelasticity acts to stabilize the current interfacial configuration: if the system is forced into an emulsified state via the external supply of energy, the mechanically generated emulsion will be stabilized against coalescence. Alternatively, if the interface is flat and undisturbed, as occurs during spontaneous emulsification, emulsion formation will be prevented. Practically, this imposes important considerations that must be adhered to if the polymer additive is used for industrial applications in crude oil processing, as it should not be introduced prior to steps involving intense turbulent mixing. For instance, the polymer can be added to crude oil during the latter stages of desalting operations, when crude oil and water are left undisturbed to separate in settling tanks.

VI. CONCLUSION

The spontaneous emulsification phenomenon in the presence of asphaltene adsorption was examined by studying the interface between water and a 1 mg/ml asphaltene-in-toluene solution. Over time, a water-in-oil emulsion begins to form near the vicinity of the liquid-liquid interface, with characteristic droplet sizes ranging between 5 and 20 μm. Experimental observations using brightfield microscopy revealed that when a polymeric flow improver, (*alt*) SNODMI, was added to the toluene solution, the onset and extent of spontaneous emulsification were almost entirely suppressed (but not eliminated) with increasing polymer fractions. Measurements of the interfacial energy per unit area showed that the polymer competitively adsorbs onto the toluene-water interface and lowers the surface energy.

These measurements were also used to elucidate the mechanism of spontaneous emulsification of asphaltenic systems. Although the presence of asphaltenes lowers the surface tension compared to a clean toluene-water interface, the energy per unit area is not vanishingly small, as required by the interfacial bending hypothesis. Additional experiments using fluorescence microscopy revealed that a diffusion and stranding process occurs, whereby diffusion of molecular across the interface and subsequent binding with asphaltene aggregates lead to the nucleation of emulsified water droplets.

Although this mechanism is a result of a chemical gradient across the bulk phases rather than a mechanical perturbation of the interface, it was shown that interfacial viscoelasticity is inversely correlated to the rate of spontaneous emulsification. Interfacial oscillatory shear and step-strain compressional rheological experiments showed that, for asphaltene-laden interfaces, the formation of an interfacial microstructure is a time-dependent phenomenon—the rate of emulsification decreases over time as the interface becomes more viscoelastic. The addition of the polymer leads to a rapid buildup of a highly viscoelasic network that hinders the emulsification phenomenon.

ACKNOWLEDGMENTS

M.R.-H. would especially like to thank Dr. Simone Bochner de Araujo for sharing her knowledge and experience on how to work with asphaltenes and for teaching how to conduct shear rheology experiments. The authors also thank Jovina Vaswani for her assistance with the shear rheology experiments. M.R.-H. acknowledges a grant from the Beijing Welltrailing Science and Technology Company. Part of this work was performed at the Stanford Nano Shared Facilities, supported by the National Science Foundation (NSF) under Award No. ECCS-1542152. Use of the Stanford Synchrotron Radiation Lightsource, SLAC National Accelerator Laboratory, is supported by the U.S. Department of Energy (DOE), Office of Science, and Office of Basic Energy Sciences under Contract No. DE-AC02-76SF00515.

APPENDIX: TENSORIAL REPRESENTATION OF THE SURFACE ENERGY FOR COMPLEX INTERFACES

Equation (5) applies to interfaces that are liquidlike in character and are unable to support a stress [29,30,32,34]. This equation can be modified for complex interfaces, where the scalar surface tension is replaced by a more complex tensorial energy per unit area $\boldsymbol{\gamma} = \gamma_s \boldsymbol{e_s e_s} + \gamma_\phi \boldsymbol{e_\phi e_\phi}$ that takes into account surfactant adsorption, curvature energies, and elastic stresses [30,42]. Here, γ_s and γ_ϕ are tangential to the s and ϕ coordinates, respectively [see Fig. 1(b)] [30,32]. For an axisymmetric drop, γ_s and γ_ϕ are functions of the height along the drop.

$$\begin{bmatrix} \gamma_\phi 0 \\ 0 \gamma_s \end{bmatrix} = \left(\gamma_0 - \Pi_{\text{ads}}(\Gamma) + \kappa \left\{ \frac{J^2}{2} - \frac{2J}{R_{sc}} \right\} + \bar{\kappa} K + \gamma^e_{\text{iso}} \right) \times \begin{bmatrix} 10 \\ 01 \end{bmatrix} + \begin{bmatrix} \gamma^e_\phi - \gamma^e_{\text{iso}} 0 \\ 0 \gamma^e_s - \gamma^e_{\text{iso}} \end{bmatrix}, \tag{A1a}$$

$$J = \frac{1}{R_\phi} + \frac{1}{R_s}, \tag{A1b}$$

$$K = \frac{1}{R_\phi R_s}, \tag{A1c}$$

where J is the mean curvature and K is the Gaussian curvature.

In the above expression, γ_0 refers to the surface tension of a clean interface. γ_0 is a thermodynamic property and is related to stretching or changes in the interfacial energy with respect to surface area at a given curvature. $\Pi_{\text{ads}}(\Gamma)$ is the surface pressure resulting from surfactant adsorption, also known as the Gibbs elasticity. This term represents the interfacial energy decrease upon adsorption of a surface active species and is dependent on the interfacial surfactant concentration Γ. $\gamma_0 - \Pi_{\text{ads}}(\Gamma)$ is the interfacial tension for a flat, nonelastic interface.

The following two terms take into account contributions to the surface energy arising from changes in the interface curvature. κ is the bending modulus (also known as a bending rigidity) and is related to changes in the interfacial energy with respect to the mean curvature J at a constant surface area and Gaussian curvature [42,47]. Conversely, $\bar{\kappa}$ is the torsional modulus and considers the changes in the interfacial energy with respect to the Gaussian curvature K at a constant surface area and mean curvature [42,47]. In practice, the torsion stress term is neglected and only the interfacial tension and bending stresses are taken into account.

The bending energy term includes contributions from the spontaneous curvature, $2/R_{sc}$. A spontaneous curvature $2/R_{sc}$ arises in certain systems when the geometrical structure of the adsorbed species is such that it can bend the interface in a manner that allows the molecules to better accommodate themselves [36,37]. Upon differentiation with respect to R, the bending term is minimized when $R = R_{sc}$. Thus, the bending rigidity κ acts as a slope and determines how strongly the interface wants to adopt its spontaneous curvature.

The bending energy contribution is important whenever microscopic systems such as the spontaneously emulsified droplets are being considered. However, for millimeter-sized pendant drops, assuming $\kappa \lesssim 100\, k_BT$ (where k_B is the Boltzmann constant) and $R_{sc} \gtrsim 1$ nm [37,46,49], then $\kappa\left(\frac{1}{R_{sc}R}\right) \lesssim 10^{-3}$ mN/m. Thus, an order-of-magnitude analysis reveals that $\gamma_0 \gg \kappa\left(\frac{1}{R_{sc}R}\right)$ and, for pendant drops, the bending energy term can be ignored.

The isotropic elastic contribution to the surface energy is given by γ^e_{iso}, and $\gamma^e_\phi - \gamma^e_{\text{iso}}$ and $\gamma^e_s - \gamma^e_{\text{iso}}$ are the deviatoric terms. The elastic energy gives rise to a nonisotropic contribution to the surface energy, which is dependent on both the strain (elastic component) and strain rate (viscous component) applied at the interface. The deviatoric elastic energy contributions must be taken into account whenever the interface is being deformed, as occurs in the compressional step-strain experiments introduced in Sec. II G. No deviatoric elastic stresses are incurred for static measurements where the interface shape does not change, such as the interfacial tension measurements using the pendant drop technique introduced in Sec. IV B 1.

REFERENCES

[1] Miller, C. A., "Spontaneous emulsification produced by diffusion—A review," Colloids Surf. **29**, 89–102 (1988).

[2] Lopez-Montilla, J. C., P. E. Herrera-Morales, S. Pandey, and D. O. Shah, "Spontaneous emulsification: Mechanisms, physiochemical aspects, modeling, and applications," J. Dispers. Sci. Technol. **23**, 219–268 (2002).

[3] de Gennes, P. G., F. Brochard-Wyart, and D. Quere, *Capillarity and Wetting Phenomena* (Springer, New York, 2004).

[4] Wilde, P., A. Mackie, F. Husband, P. Gunning, and V. Morris, "Proteins and emulsifiers at liquid interfaces," Adv. Colloid Interface Sci. **108–109**, 63–71 (1993).

[5] Solans, C., D. Morales, and M. Homs, "Spontaneous emulsification," Curr. Opin. Colloid Interface Sci. **22**, 88–93 (2016).

[6] Vitale, S. A., and J. L. Katz, "Liquid droplet dispersions formed by homogeneous liquid-liquid nucleation: 'The ouzo effect'," Langmuir **19**, 4105–4110 (2003).

[7] Davies, J. T., "Mass-transfer and interfacial phenomena," Adv. Chem. Eng. **4**, 1–50 (1964).

[8] Ruschak, K. J., and C. A. Miller, "Spontaneous emulsification in ternary systems with mass transfer," Ind. Eng. Chem. Fundam. **11**, 534–540 (1972).

[9] Bochner de Araujo, S., M. Merola, D. Vlassopoulos, and G. G. Fuller, "Droplet coalescence and spontaneous emulsification in the presence of asphaltene adsorption," Langmuir **33**, 10501–10510 (2017).

[10] Duboué, J., M. Bourrel, A. Santanach Carreras, E. Klimenko, N. Agenet, N. Passade-Boupat, and F. Lequeux, "Auto-emulsification of water at the crude oil/water interface: A mechanism driven by osmotic gradient," Energy Fuels **33**, 7020–7027 (2019).

[11] Chang, C. C., A. Nowbahar, V. Mansard, I. Williams, J. Mecca, A. K. Schmitt, T. C. Kalantar, T. H. Kuo, and T. M. Squires, "Interfacial rheology and heterogenity of aging asphaltene layers at the water-oil interface," Langmuir **34**, 5409–5415 (2018).

[12] Mohammed, R. A., A. I. Bailey, P. F. Luckham, and S. E. Taylor, "Dewatering of crude oil emulsions 1. Rheological behaviour of the crude oil-water interface," Colloids Surf. A **80**, 223–235 (1993).

[13] Bochner de Araujo, S., M. Reyssat, C. Monteux, and G. G. Fuller, "Ablation of water drops suspended in asphaltene/heptol solutions due to spontaneous emulsification," Sci. Adv. **5**, eaax8227 (2019).

[14] Sun, M., K. Mogensen, M. Bennetzen, and A. Firoozabadi, "Demulsifier in injected water for improved recovery of crudes that form water/oil emulsions," Soc. Pet. Eng. J. **19**, 1–9 (2016).

[15] Xu, X., J. Yang, and J. Gao, "Effects of demulsifier structure on desalting efficiency of crude oils," Pet. Sci. Technol. **24**, 673–688 (2006).

[16] Davies, J. T., and E. K. Rideal, *Interfacial Phenomena* (Academic, New York, 1961).

[17] Freer, E. M., and C. J. Radke, "Relaxation of asphaltenes at the toluene/water interface: Diffusion exchange and surface rearrangement," J. Adhes. **80**, 481–496 (2004).

[18] Mullins, O. C., "The modified Yen model," Energy Fuels **24**, 2179–2207 (2010).

[19] Mullins, O., H. Sabbah, J. Eyssautier, A. E. Pomerantz, L. Barre, A. B. Andrews, Y. Ruiz-Morales, F. Mostowfi, R. McFarlane, L. Goual, R. Lepkowicz, T. Cooper, J. Orbulescu, R. M. Leblanc, J. Edwards, and R. N. Zare, "Advances in asphaltene science and the Yen-Mullins model," Energy Fuels **26**, 3986–4003 (2012).

[20] Eyssautier, J., D. Frot, and L. Barre, "Structure and dynamic properties of colloidal asphaltene aggregates," Langmuir **28**, 11997–12004 (2012).

[21] Kuznicki, T., J. H. Masliyah, and S. Bhattacharjee, "Aggregation and partitioning of model asphaltenes at toluene-water interfaces: Molecular dynamics simulations," Energy Fuels **23**, 5027–5035 (2009).

[22] Eyssautier, J., P. Levitz, D. Espinat, J. Jestin, J. Gummel, I. Grillo, and L. Barre, "Insight into asphaltene nanoaggregate structure inferred by small angle neutron and x-ray scattering," J. Phys. Chem. B **115**, 6827–6837 (2011).

[23] Langevin, D., and J. F. Argillier, "Interfacial behavior of asphaltenes," Adv. Colloid Interface Sci. **233**, 83–93 (2016).

[24] ASTM, "Standard test method for characteristic groups in rubber extender and processing oils and other petroleum derived oils by clay-gel absorption chromatographic method," A. D2007-03, 2003.

[25] Cao, K., Q. Zhu, X. Wei, Y. Yu, and Z. Yao, "Influences of the molecular weight and its distribution of poly(styrene-alt-octadecyl maleimide) as a flow improver for crude oils," Energy Fuels **30**, 2721–2728 (2016).

[26] Cao, K., Q. Zhu, X. Wei, and Z. Yao, "Study on the influence of the imidization degree of poly(styrene-co- octadecyl maleimide) as a flow improver in waxy crude oils with asphaltenes," Energy Fuels **29**, 993–1000 (2015).

[27] Cao, K., X. Wei, B. Li, J. Zhang, and Z. Yao, "Study of the influence of imidization degree of poly(styrene-co-octadecyl maleimide) as waxy crude oil flow improvers," Energy Fuels **27**, 640–645 (2012).

[28] Rotenberg, Y., L. Boruvka, and A. W. Neumann, "Determination of surface tension and contact angle from the shapes of axisymmetric fluid interfaces," J. Colloid Interface Sci. **93**, 169–183 (1983).

[29] Berry, J. D., M. J. Neeson, R. R. Dagastine, D. Y. C. Chan, and R. F. Tabor, "Measurement of surface and interfacial tension using pendant drop tensiometry," J. Colloid Interface Sci. **454**, 226–237 (2015).

[30] Nagel, M., T. A. Tervoort, and J. Vermant, "From drop-shape analysis to stress-fitting elastometry," Adv. Colloid Interface Sci. **247**, 33–51 (2017).

[31] Vandebril, S., A. Franck, G. G. Fuller, P. Moldenaers, and J. Vermant, "A double wall-ring geometry for interfacial shear rheometry," Rheol. Acta **49**, 131–144 (2010).

[32] Danov, K. D., R. D. Stanimirova, P. A. Kralchevsky, K. G. Marinova, N. A. Alexandrov, S. D. Stoyanov, T. B. J. Blijdenstein, and E. G. Pelan, "Capillary meniscus dynamometry—Method for determining the surface tension of drops and bubbles with isotropic and anisotropic surface stress distributions," J. Colloid Interface Sci. **440**, 168–178 (2015).

[33] Kannan, A., I. C. Shieh, D. L. Leiske, and G. G. Fuller, "Monoclonal antibody interfaces: Dilatation mechanics and bubble coalescence," Langmuir **34**, 630–638 (2018).

[34] Carvajal, D., E. J. Laprade, K. J. Henderson, and K. R. Shull, "Mechanics of pendant drops and axisymmetric membranes," Soft Matter **7**, 10508–10519 (2011).

[35] De Gennes, P. G., and C. Taupin, "Microemulsions and the flexibility of oil/water interfaces," J. Phys. Chem. **86**, 2294–2304 (1982).

[36] Leung, R., and D. O. Shah, "Solubilization and phase equilibria of water-in-oil microemulsions: I. Effects of spontaneous curvature and elasticity of interfacial films," J. Colloid Interface Sci. **120**, 320–329 (1987).

[37] Kabalnov, A., and H. Wennerstrom, "Macroemulsion stability: The oriented wedge theory revisited," Langmuir **12**, 276–292 (1996).

[38] Hermans, E., S. Bhamla, P. Kao, G. G. Fuller, and J. Vermant, "Lung surfactants and different contributions to thin film stability," Soft Matter **11**, 8048–8057 (2015).

[39] Aldousary, S., and A. R. Kovscek, "The diffusion of water through oil contributes to spontaneous emulsification T during low salinity waterflooding," J. Pet. Sci. Eng. **179**, 606–614 (2019).

[40] Quintanar-Guerrero, D., E. Allemann, E. Doelker, and H. Fessi, "A mechanistic study of the formation of polymer nanoparticles by the emulsification-diffusion technique," Colloid Polym. Sci. **275**, 640–647 (1997).

[41] Miller, C. A., R. N. Hwan, W. J. Benton, and T. Fort, "Ultralow interfacial tensions and their relation to phase separation in micellar solutions," J. Colloid Interface Sci. **61**, 554–568 (1976).

[42] Murphy, C. L., Thermodynamics of low tension and highly curved interfaces, Ph.D. thesis, University of Minnesota, Minneapolis, MN, 1966.

[43] Miller, C. A., and P. Neogi, "Thermodynamics of microemulsions: Combined effects of dispersion entropy of drops and bending energy of surfactant films," AIChE J. **26**, 212–220 (1980).

[44] Helfrich, W., "Elastic properties of lipid bilayers: Theory and possible experiments," Z. Naturforsch. **28c**, 693–703 (1973).

[45] Miller, C. A., "Interfacial bending effects and interfacial tensions in microemulsions," J. Dispers. Sci. Technol. **6**, 159–173 (1985).

[46] Kellay, H., B. P. Binks, Y. Hendrikx, L. T. Lee, and J. Meunier, "Properties of surfactant monolayers in relation to microemulsion phase behavior," Adv. Colloid Interface Sci. **49**, 89–112 (1994).

[47] Leermakers, F. A. M., P. A. Barneveld, J. Sprakel, and N. A. M. Besseling, "Symmetric liquid-liquid interface with a nonzero spontaneous curvature," Phys. Rev. Lett. **97**, 066103 (2006).

[48] Leung, R., and D. O. Shah, "Solubilization and phase equilibria of water-in-oil microemulsions: II. Effects of alcohols, oils, and salinity on single-chain surfactant systems," J. Colloid Interface Sci. **120**, 330–344 (1987).

[49] Meunier, J., "Measurement of the rigidity coefficient of a surfactant layer and structure of the oil or water microemulsion interface," J. Phys. Lett. **46**, L–1005–L–1014 (1985).

[50] Ruckenstein, E., and J. C. Chi, "Stability of microemulsions," J. Chem. Soc. Faraday Trans. 2 **71**, 1690–1707 (1975).

[51] Sánchez-Puga, P., J. Tajuelo, J. M. Pastor, and M. A. Rubio, "Dynamic measurements with the bicone interfacial shear rheometer: Numerical bench-marking of flow field-based data processing," Colloids Interfaces **2**(4), 69 (2018).

[52] Verwijlen, T. P., P. Moldenaers, H. A. Stone, and J. Vermant, "Study of the flow field in the magnetic rod interfacial stress rheometer," Langmuir **27**, 9345–9358 (2011).

[53] Freer, E. M., T. Svitova, and C. J. Radke, "The role of interfacial rheology in reservoir mixed wettability," J. Pet. Sci. Eng. **39**, 137–158 (2003).

[54] See supplementary material at https://doi.org/10.1122/1.5145307 for the asphaltene absorbance spectra, fluorescence microscopy control experiments, curvature profiles for the pendant drop method, amplitude sweeps for the oscillatory shear rheology experiments, and validation for the compressional modulus calculations.